Supplementary material

Enhancing the mechanical and antibacterial properties of hydroxyapatite bioceramics by in-situ graphene doping to promote osteointegration infected bone defect

Qipeng Li[1], Hao Shi[2], Yuyi Wang[2], Ruitao Hu[3], Cong Feng[2], Xiaodong Ma[4], Ye Wang[1]*, Xiangfeng Li[2]*, Xiangdong Zhu[2], Xingdong Zhang[2]

1 College of Chemical Engineering, Sichuan University, Chengdu, 610065, China

2 National Engineering Research Center for Biomaterials, College of Biomedical Engineering, Sichuan University, Chengdu, 610065, China

3 Pittsburgh Institute, Sichuan University, Chengdu, 610065, China

4 School of Chemical Engineering, University of Queensland, Brisbane, QLD, 4072, Australia

*Corresponding authors E-mail: wangye@scu.edu.com (Y. Wang);
hkdlixiangfeng@163.com (X.F. Li)

Supplementary material

Table S1. Table of primers utilized for qRT-PCR amplification

Gene	5' to 3	Primers
Alp	Sense	5'-ATCTTTGGTCTGGCTCCCATG-3'
	Anti-Sense	5'-TTTCCCGTTCACCGTCCAC-3'
Runx2	Sense	5'-AGCCTCTTCAGCGCAGTGAC-3'
	Anti-Sense	5'-CTGGTGCTCGGATCCCAAA-3'
Osx	Sense	5'-ACAGACGAACAACCCAAACT-3'
	Anti-Sense	5'-GGTTTTTGGTCACGTTCAGT-3'
Col-1	Sense	5'- ACAGACGAACAACCCAAACT-3'
	Anti-Sense	5'- GGTTTTTGGTCACGTTCAGT-3'
Ocn	Sense	5'-CCTCTCTCTGCTCACTCTGCTG-3'
	Anti-Sense	5'-ACCTTACTGCCCTCCTGCTTG-3'
Opn	Sense	5'-TCTGATGAGACCGTCACTGC-3'
	Anti-Sense	5'-AGGTCCTCATCTGTGGCATC-3'
Gapdh	Sense	5'-TGGTGAAGGTCGGTGTGAAC-3'
	Anti-Sense	5'-CCATGTAGTTGAGGTCAATGAAGG-3'

Figure S1. The volume shrinkage of HA, HA-0.1%FLG, HA-0.5%FLG, HA-1%FLG after vacuum sintering.

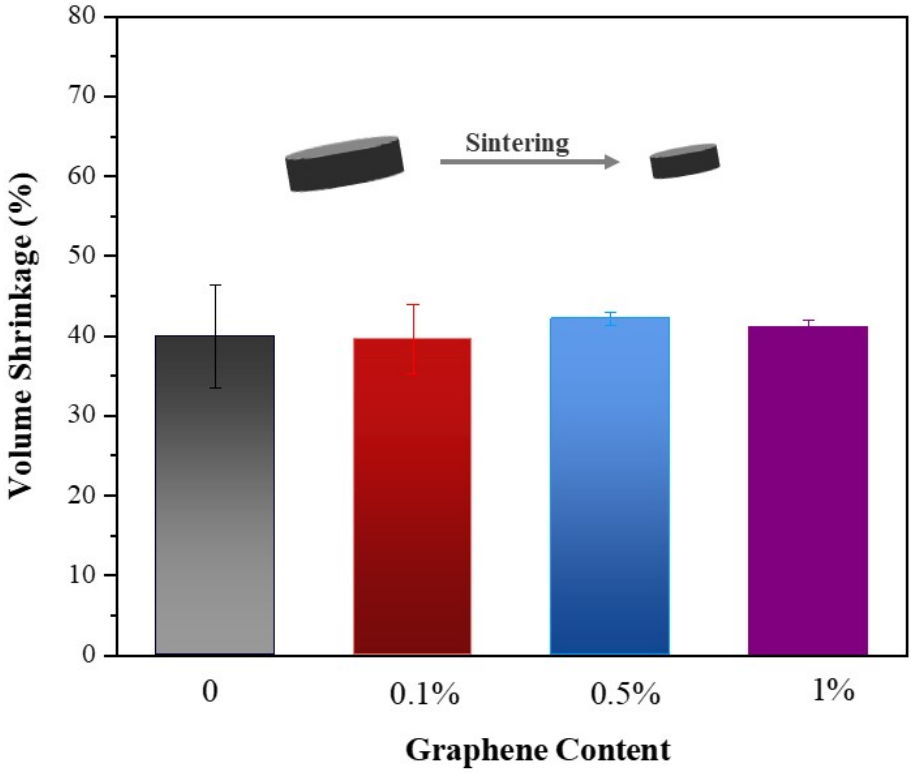

By measuring the cylindrical HA ceramic sizes before and after vacuum sintering, volume shrinkage of HA, HA-0.1%FLG, HA-0.5%FLG, HA-1%FLG were calculated by the geometric method. All data are presented as mean ± standard deviation (SD). At least three samples were used for each group. As shown in **Figure S1**, The volume shrinkage rate of HA, HA-0.1%FLG, HA-0.5%FLG, HA-1%FLG were 39.95±6.50%, 39.57±4.30%, 42.13±0.81%, 41.10±0.81% respectively. It did not show significant difference for volume shrinkage rate of four groups. The volume shrinkage ratio of HA-0.5%FLG and HA-1%FLG were bigger, which may be related to the amount of doped graphene.

Figure S2. The TG curve of HA-1%FLG in air atmosphere.

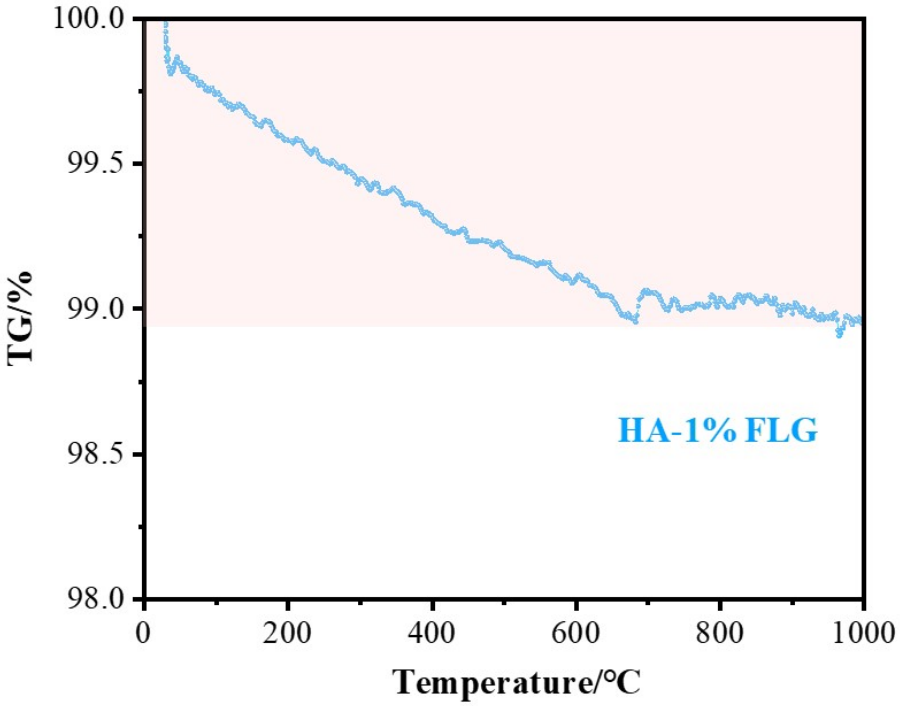

The wight curve of HA-1%FLG was analyzed with TG method in air atmosphere with heating rate of 5 ℃/min (STS 449F3, NETZSCH, Germany). As shown in **Figure S2**, the final weight loss of HA-1%FLG was 1%, which was consistent with the doped graphene mass. Since graphene was easily oxidized in air, it greatly increased the difficulty of preparing graphene composite bioceramics, which was the reason that we adopted vacuum sintering in this study.

Figure S3. Graphene binding stability with HA of composite bioceramic. a) The

appearances of HA, HA-0.1%FLG, HA-0.5%FLG, HA-1%FLG after 30 min ultrasonic treatment in ultrapure water. b) The ultraviolet-visible absorption wave intensity of HA, HA-0.1%FLG, HA-0.5%FLG, HA-1%FLG solution after 30 min ultrasonic treatment in ultrapure water.

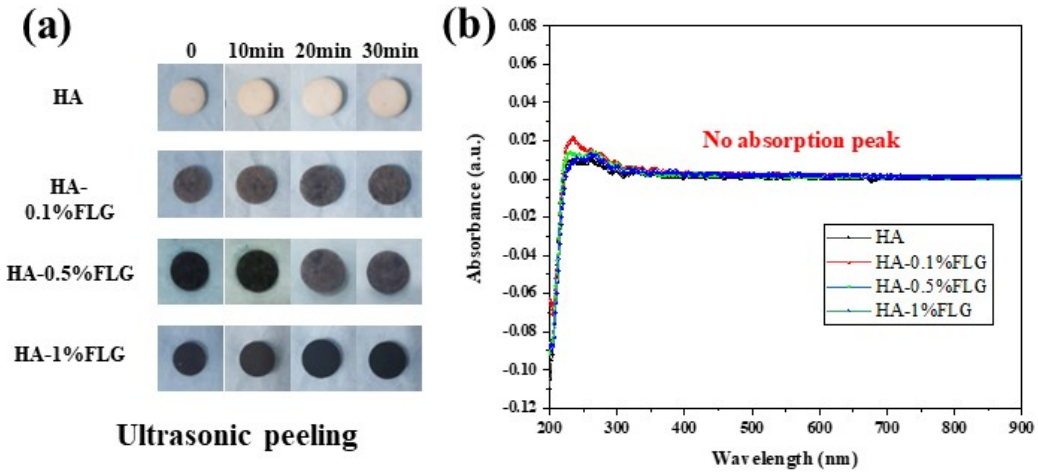

The absorption wave intensity of samples after 30 min ultrasonic treatment in ultrapure water was measured by Ultraviolet-visible Spectrophotometer (UV752N), to characterize the stability of the composite structure with graphene. The appearance of the four samples did not change significantly with increasing ultrasonic peeling time and no exfoliated graphene was observed, as shown in the **Figure S3a**. We found that no obvious carbon peak existed in solution after 30 min ultrasonic treatment (**Figure S3b**), proving the strong connectivity of graphene in the composite structure. The results clarified that the high stability of graphene composite bioceramics *in situ* synthesis compared with surface adsorption and deposition methods.

Figure S4. Crack fracture patterns of HA and cross-sectional images of HA-0.5%FLG

and HA-1%FLG at different magnifications.

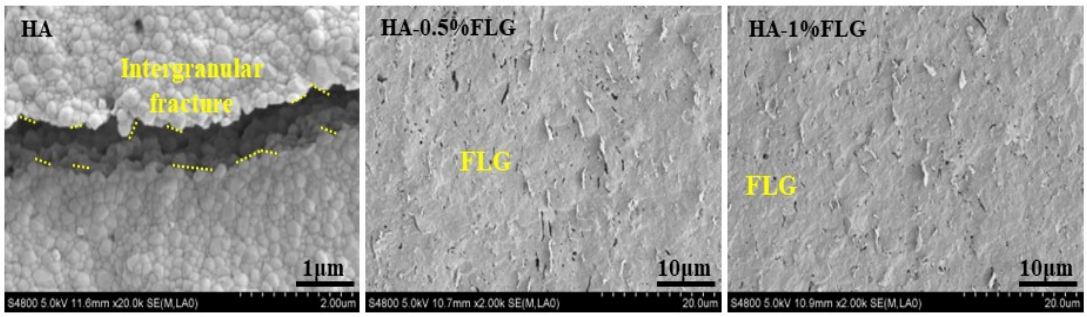

As an illustration and supplement to **Figure 2a**, it can be clearly seen that the fracture mode of pure HA is mainly intergranular fracture in **Figure S4**. At the same time, under the small magnification, a large amount of graphene with uniform distribution can be observed in cross-sectional images of HA-0.5%FLG and HA-1%FLG. The results verified that the strategy of equipartition and dispersion of graphene into the bioceramic matrix is successful.

Figure S5. Compressive strength and compressive modulus of HA, HA-0.1%FLG,

HA-0.5%FLG, HA-1%FLG.

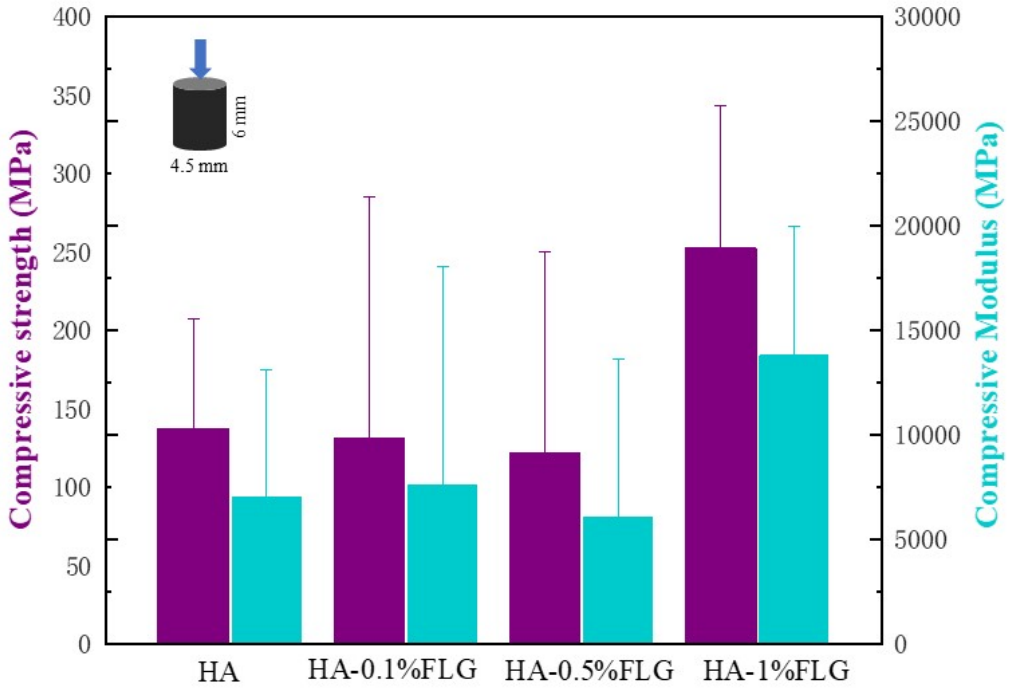

Compressive strength and compressive modulus of HA, HA-0.1%FLG, HA-0.5%FLG, HA-1%FLG were obtained by a universal testing machine (Autograph AG-X, Japan). As shown in the **Figure S5**, compressive strength of HA, HA-0.1%FLG, HA-0.5%FLG were almost the same, but compressive strength of HA-1%FLG was improved, as well as the trend of compressive modulus. The results showed that graphene could improve the compressive strength and modulus of HA, but its concentration needed to be increased. The graphene with low concentration in the bioceramic matrix had a limited effect on increasing the stiffness, even the stiffness will be reduced.

Figure S6. Experimental procedure diagram of implantation and photothermal

antibacterial experiment for HA-0.5%FLG in rabbit femur.

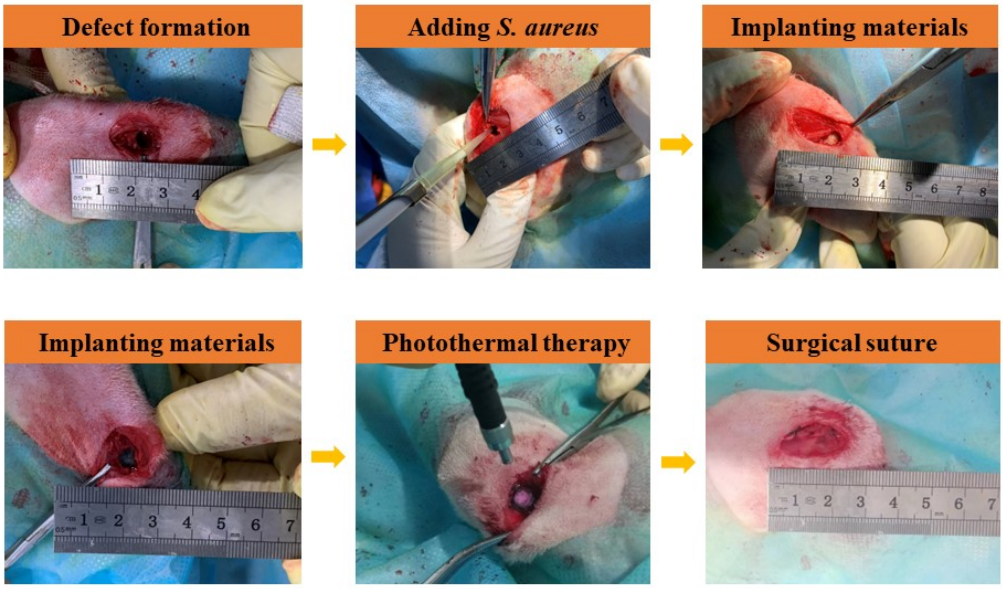

The experimental procedures for the establishment of the in vivo animal model were shown in **Figure S6**. A cylindrical hole (Φ 3 mm × 4 mm) was drilled perpendicularly to the distal femur at a slow speed with saline solution irrigation to avoid thermal necrosis. Then 10 μL *S. aureus* suspension was quickly added, following HA and HA-0.5%FLG were implanted, respectively. They were irradiated with NIR (808 nm, 1 W cm^{-2}) for 5 minutes and the temperature change values were recorded (**Figure 6c**). Finally, we performed postoperative wound suturing and the rabbits were fed for two months. After 3, 5 and 7 days of operation, NIR irradiation was also performed on the implanting position to achieve better long-term antibacterial effect.

Figure S7. GIF of intraoperative real-time temperature of HA-0.5%FLG at the power

1.0W cm^{-2}.

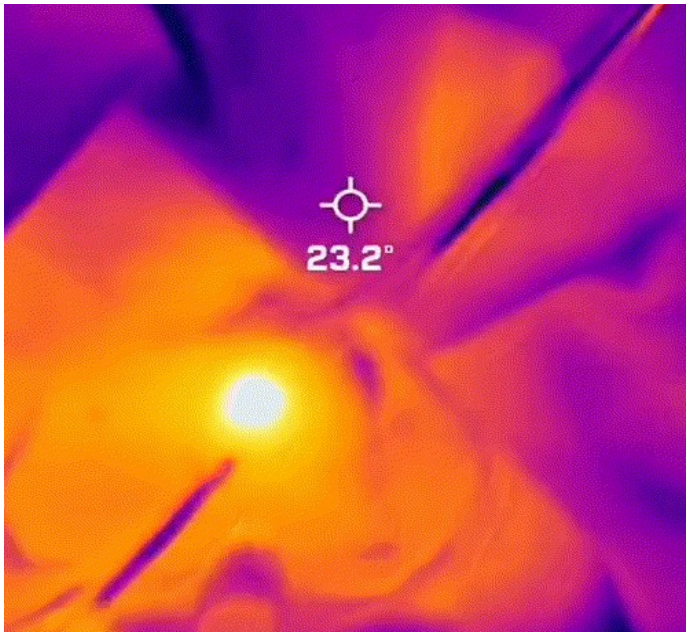

The implants were irradiated by NIR (808 nm, 1.0W cm^{-2}) for 8 s and the real-time temperature changes were captured into **Figure S7**. This helped us more intuitive understanding in terms of the HA-0.5%FLG temperature response to irradiation. From **Figure S7**, we could see that the surface temperature of the scaffolds will increase rapidly after the alignment of the irradiated material. And the temperature curves of 5 minutes were shown in **Figure 6C**. Compared with HA, the temperature HA-0.5%FLG could keep high temperature state (over 50 ℃) in 5 minutes, which could effectively kill *S. aureus*.

Figure S8. a) The rabbit femurs were cut to obtain the material containing scaffolds

after two months. b) The new bone volume to tissue volume ratio (BV/TV). Values are expressed as the mean ± SD (n = 3); *p < 0.05.

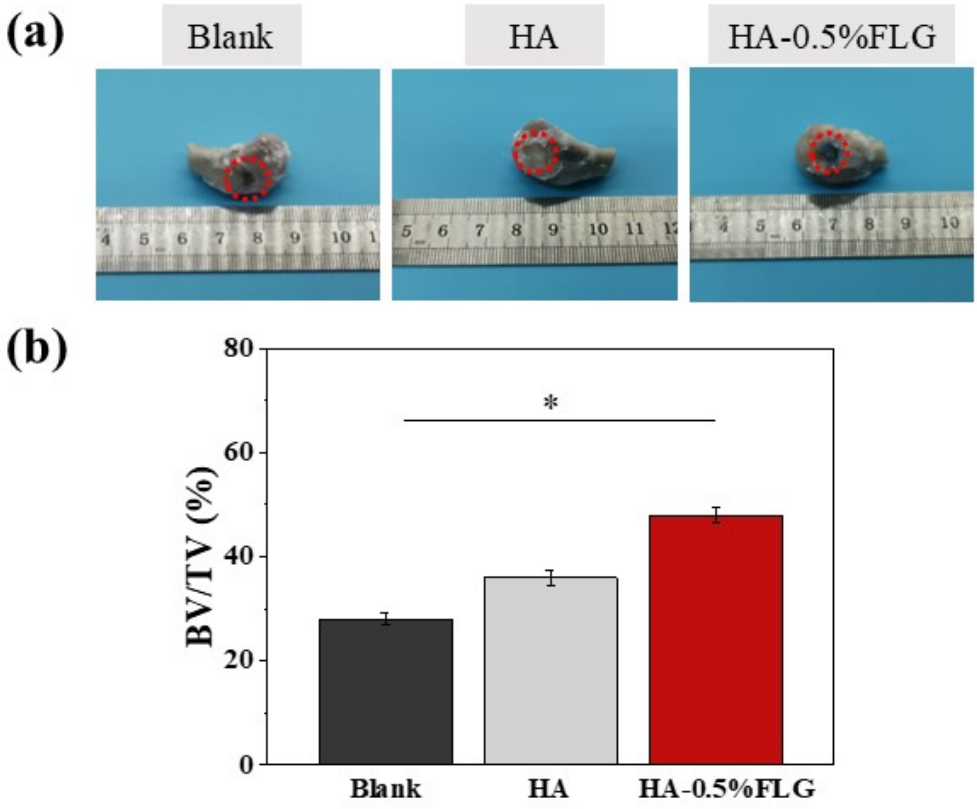

Two months later, all rabbits were euthanized by an intraperitoneal overdose injection of sodium pentobarbital. The rabbit femurs containing implanted material were obtained. The implantations were immediately fixed in 4 % paraformaldehyde solution, and then scanned by micro-CT. As shown in **Figure S8**, defects and implant materials were subsequently exposed to obtain in vivo antibacterial results and new bone growth was analyzed by reconstruction. We could clearly see that there was no obvious defect in the place where scaffolds were implanted, and the integration with the surrounding bone growth was very good. The new bone to tissue volume ratio of HA-0.5%FLG also showed a significant difference.